

Néel and Valence Bond Crystal Order on a Distorted Kagomé Lattice: Implications For Zn-Paratacamite

Erik S. Sørensen,¹ Michael J. Lawler,^{2,3} and Yong Baek Kim⁴

¹*Department of Physics and Astronomy, McMaster University, Hamilton, Ontario, Canada L8S 4M1**

²*Department of Physics, Applied Physics and Astronomy, Binghamton University, PO Box 6000, Binghamton, NY 13902-6000*

³*Department of Physics, Cornell University, Ithaca, NY 14853*

⁴*Department of Physics, University of Toronto, Toronto, Ontario M5S 1A7, Canada*

(Dated: December 3, 2018)

Zn-Paratacamite is a rare spin 1/2 antiferromagnetic insulator with an ideal kagomé lattice structure in part of its phase diagram. As a function of Zn doping, this material undergoes a structural distortion which relieves the frustration and introduces magnetic order in the ground state, though the precise nature of the order is not clear at this point. In this paper, we present strong evidence for Néel ordering in the *strongly* distorted phase of Zn-Paratacamite through the application of quantum Monte-Carlo techniques. These numerical results support a recent Schwinger-boson mean field theory of Zn-Paratacamite. For *weak* distortion, close to the ideal kagomé limit, our results indicate a regime with no Néel order but with a broken glide-plane symmetry. For this model the glide-plane symmetry is broken by *any* valence bond crystal. Hence, our results lend support to recent proposals^{1,2} of a valence bond crystal ground state for the undistorted lattice. The phase transition between the two phases could be in the deconfined universality class if it is not a first order transition.

PACS numbers: 75.10.Jm, 73.43.Nq, 75.40.Mg

I. INTRODUCTION

Recently, a number of spin 1/2 frustrated magnetic insulators have been discovered without any sign of magnetic order or structural distortions down to the lowest temperatures studied^{3,4,5,6}. Among these materials, the Zn doped Paratacamite family stands out for having a (nearly) controllable degree of distortion allowing the amount of geometric frustration to be tuned directly by an experimentalist. As such, they are a promising place to look for new phases of matter while at the same time probe how these new phases may be related to more well understood phases.

The control of the distortion is largely through the chemical pressure induced by the substitution of Zn atoms for Cu atoms on the (grey) triangular lattice planes that live in between kagomé-planes, as shown in Fig. 1. While Zn and Cu atoms are similar in size, Zn atoms fit into these sites without disrupting their environment, unlike Cu atoms which distort the kagomé plans given a high enough density. In particular, for less than 0.3 filling of Zn atoms (greater than 0.7 filling of Cu atoms) the lattice distorts in a remarkable bi-partite structure and magnetic order is found in the ground state^{5,7,8}. The spins are thus relatively unfrustrated at these low doping concentrations. For Zn doping larger than this threshold, the lattice has the undistorted ideal kagomé form and for $x \geq 0.4$ no magnetic ordering has been reported down to 50 mK despite an estimated spin exchange $J \sim 200K$ ⁷.

A natural theoretical model of this material is the spin 1/2 Heisenberg model with two exchange parameters on

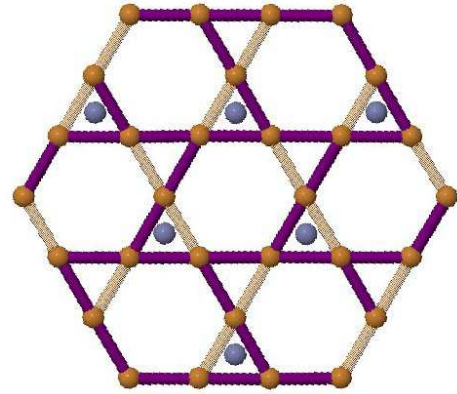


FIG. 1: (Color online) The layered Zn Paratacamite magnetic lattice structure. Cu atoms live on the (sometimes distorted) kagomé layer (bronze atoms) while Zn or Cu atoms occupy sites on a triangular lattice above the kagomé plane (grey atoms). Solid (purple) bonds represent nearest neighbors ($\langle\langle ij \rangle\rangle$ in Eq. (1)) resulting in a ‘brick-wall’ lattice, while transparent (bronze) bonds represent the next nearest neighbors ($\langle\langle ij \rangle\rangle$ in Eq. (1)).

a distorted kagomé lattice^{7,8,9} (see Fig. 1):

$$H = J \sum_{\langle i,j \rangle} \mathbf{S}_i \cdot \mathbf{S}_j + \lambda_D J \sum_{\langle\langle ij \rangle\rangle} \mathbf{S}_i \cdot \mathbf{S}_j \quad (1)$$

Here λ_D tunes the distortion on the next nearest neighbor bonds (nnn) with $\lambda_d = 1$ the undistorted ideal kagomé limit (where nnn bonds are equivalent to nn bonds). This

is an idealized model for several reasons: it assumes the coupling between planes and further neighbors is weak (which seems reasonable^{7,8}), it neglects Dzyaloshinsky-Moria interactions possibly important for the low temperature susceptibility^{10,11}, and it replaces the effect of doping in the triangle lattice planes with the uniform distortion parameter λ_D . While it is possible that any of these approximations may be important for some properties of Zn Paratacamite, here we will focus on those properties which clearly belong to the phenomenology of this simplified model.

In this paper, we study the ground state properties of the Hamiltonian in Eq. (1) as a function of λ_D , extrapolating between a bi-partite ‘brick-wall’ lattice at $\lambda_D = 0$ and the isotropic kagomé lattice at $\lambda_D = 1$. At $\lambda_D = 0$, we show using valence bond quantum Monte-Carlo^{12,13}, that the ground state is magnetically ordered with the expected Néel pattern for this bi-partite lattice and with a magnetization of $m^\dagger = 0.240(1)$ that is 22% smaller than the square lattice value¹⁴. For $0 \leq \lambda_D \leq 1$ we study this model using exact diagonalization on finite size clusters of size 12, 24 and 36 sites. By introducing symmetry breaking fields, we study the susceptibility of the ground state towards dimerization. Remarkably, we find that for $\lambda_D \gtrsim 0.8$, a phase transition occurs towards a rotationally invariant state which prefers to have a broken glide-plane symmetry, consistent with the presence of a VBC order including the pin-wheel VBC pattern proposed by Ref. 9. This symmetry breaking survives up to the $\lambda_D = 1$ ideal kagomé limit. While it is difficult to draw definitive conclusions on such small systems, a broken glide-plane symmetry support Refs. 1,2,15 proposal that the spin 1/2 kagomé antiferromagnet has a valence bond crystal (VBC) ground state. At the same time a broken glide-plane symmetry is not consistent with a spin-liquid phase, frequently supported by other exact diagonalization studies¹⁶. In addition, while we can’t rule out a first order transition from a VBC phase to the Néel phase in our model, it is also possible this quantum phase transition is in the deconfined universality class¹⁷.

II. RESULTS AT $\lambda_D = 0$

We first discuss our results obtained at $\lambda_D = 0$ where we have been able to study large system. As can be seen from Figs. 1, where the transparent (bronze) bonds are proportional to λ_D , the lattice formed by the remaining solid (purple) bonds is a bi-partite ‘brick-wall’ lattice with a coordination number of 3 on two thirds of the sites and of 2 on the remaining sites. Due to the bi-partite nature of the $\lambda_D = 0$ lattice there is no frustration. A classical AF Néel state can be unambiguously assigned to the lattice. It is then possible to perform very efficient quantum Monte Carlo simulations using the recently proposed^{12,13} valence bond quantum Monte Carlo (VBQMC). For $\lambda_D = 0$ there is no sign problem and extremely precise results can be obtained.

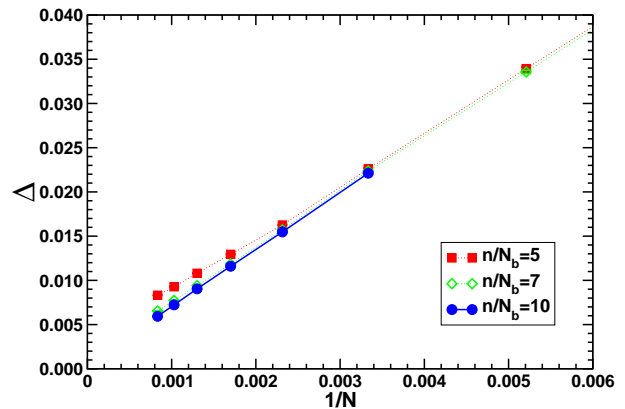


FIG. 2: (Color online.) The singlet-triplet gap, Δ , versus inverse system size $1/N$. The different curves correspond to different expansion orders n , with the ratio n/N_b kept fixed. Here, N_b is the number of bond operators in the Hamiltonian, $N_b = (4/3)N$. Results are shown for $n/N_b = 5$ (■), $n/N_b = 7$ (◇), $n/N_b = 10$ (●). Error bars are shown but are typically smaller than the symbols.

VBQMC is a projection method where the $T = 0$ ground-state is projected out through the repeated application of the hamiltonian, H , on a trial state, $|\Psi_T\rangle$. In essence, $|\Psi_G\rangle = (-H)^n |\Psi_T\rangle$. In the limit where $n \rightarrow \infty$ this becomes exact. In a practical implementation n is kept fixed at a high number and the different terms in $|\Psi_G\rangle$ are sampled using Monte Carlo methods. For convergence, the relevant lattice size independent expansion order is n/N_b where N_b is the number of terms in the Hamiltonian. N_b is equal to $(4/3)N$ for the brick-wall lattice with N the number of sites in the lattice. Typically we use $n/N_b = 3 - 10$ and an extrapolation to $n/N_b = \infty$ can then be performed.

We have performed systematic VBQMC studies of $\lambda_D = 0$ brick-wall lattices with number of sites $N = 12 \times m^2$ for $m = 1, \dots, 10$ using periodic boundary conditions. Typically, $10^6 - 10^7$ MCS were performed for a range of values of $n/N_b = 3, 5, 7, 10$. All errorbars were calculated using standard binning techniques.

A very natural question to ask is if the $\lambda_D = 0$ brick-wall lattice has a non-zero singlet to triplet gap, Δ . A particularly appealing feature of VBQMC is that it allows for a direct estimator^{12,13} of this gap independent of the estimators for the ground-state singlet and excited triplet energies. Due to a cancellation of errors it is then possible to calculate this gap with a precision significantly exceeding that which could have been obtained by separately calculating the ground and excited state energies. Our results for Δ at $\lambda_D = 0$ are shown in Fig. 2. Data are shown for 3 different values of $n/N_b = 5$ (■), $n/N_b = 7$ (◇), $n/N_b = 10$ (●) versus inverse system size $1/N$. At $N = 1200$, $n/N_b = 10$ the gap is $\Delta = 0.0059(1)J$ and minimal dependence on the expansion order n/N_b is seen. From the results shown in Fig. 2 we conclude that the gap vanishes in the thermodynamic

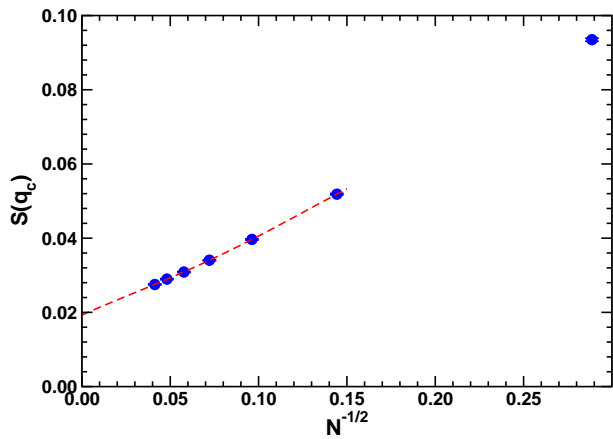


FIG. 3: (Color online.) The structure factor, $S(\mathbf{q}_c)$, versus inverse linear system size $1/\sqrt{N}$. Results are shown for $n/N_b = 10$. Error bars are shown but are typically smaller than the symbols. Results for $n/N_b = 7$ are indistinguishable from the $n/N_b = 10$ results shown and have been left out for clarity.

limit.

For the two-dimensional square lattice anti-ferromagnetic Heisenberg model it is well known¹⁸ that the anti-ferromagnetic order exists at $T = 0$ with $m^\dagger = 0.30743(1)$ ¹⁴. The square lattice has a coordination number of 4 whereas the brick-wall lattice has a mixed coordination of 2 and 3. We therefore expect m^\dagger to be smaller or possibly zero for the brick-wall lattice. As usual, we define:

$$S(\mathbf{q}_c) = \frac{1}{N^2} \left\langle \left(\sum_{x,y} \tilde{S}^z(x,y) \right)^2 \right\rangle, \quad (2)$$

where \mathbf{q}_c is the wave-vector of the staggered magnetization and $\tilde{S}^z(x,y)$ is given by:

$$\tilde{S}^z(x,y) = \frac{1}{2} \epsilon_{x,y} \sigma^z(x,y), \quad (3)$$

with $\epsilon_{x,y}$ equal to +1 or -1 depending on what sublattice the point (x,y) belongs to. Hence we have¹⁸:

$$m^\dagger = \langle \tilde{S}_i^z \rangle = \lim_{L \rightarrow \infty} \sqrt{3S(\mathbf{q}_c)} \quad (4)$$

Our results for $S(\mathbf{q}_c)$ for $n/N_b = 10$ are shown in Fig. 3. It is expected¹⁸ that the leading finite size corrections are of the form $1/\sqrt{N}$ and a fit to this form yields $S(\mathbf{q}_c) = 0.0192(5)$ and consequently:

$$m^\dagger = 0.240(3). \quad (5)$$

As expected, this value is reduced with respect to the square lattice result, but is clearly non-zero, indicating a well established anti-ferromagnetic order at $\lambda_D = 0$.

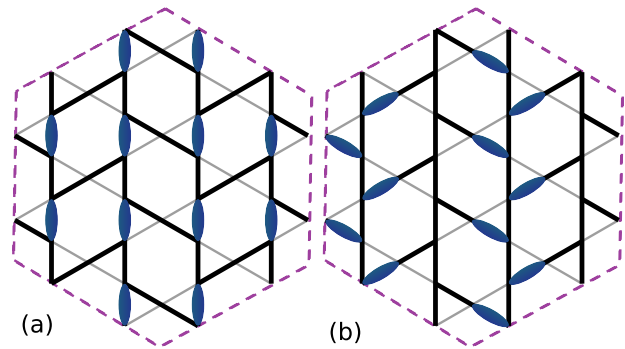


FIG. 4: (Color online.) (a) The glide-plane symmetry breaking field. (b) C_2 symmetry breaking field. Solid dimers denote bonds where the coupling strength is modified to J' .

III. RESULTS AT $\lambda_D \neq 0$

We now turn to a discussion of our results for $0 < \lambda_D \leq 1$. In this case it is no longer possible to perform VBQMC calculations due to a sign problem that appears rather severe as soon as $\lambda_D \neq 0$ and reliable numerical results are therefore much harder to obtain. In light of the strong sign problem we have performed exact diagonalization studies for $0 < \lambda \leq 1$ on finite size systems employing periodic boundary conditions. Our goal is to study generalized bond susceptibilities with respect to symmetry breaking fields. We focus on C_2 and glide-plane (GP) symmetry breaking fields shown in Fig. 4 where the dimers indicate bonds where the strength is modified $J' = J \pm \delta$. The C_2 symmetry corresponds to a rotation by π and clearly the field shown in Fig. 4(a) breaks this symmetry. The GP symmetry⁹ is somewhat more exotic and corresponds to a translation along the rails where the dimers are sitting followed by a reflection around one of these rails. We note that the GP field does not break the C_2 symmetry and likewise the C_2 field preserves the GP symmetry. The pin-wheel VBC discussed in Ref. 9 would break the GP symmetry but not the C_2 symmetry where as the columnar VBC⁹ would break both. If we by $\mathbf{b}, \mathbf{b}_{C_2,GP}$ denote the ground-state expectation value $\langle \mathbf{S}_i \cdot \mathbf{S}_j \rangle$ for the bond \mathbf{b} and its partner under the symmetry operation $\mathbf{b}_{C_2,GP}$, we can define the generalized bond susceptibility as follows:

$$\chi_{C_2,GP} = \lim_{\delta \rightarrow 0} \frac{|\Delta \mathbf{b}_{C_2,GP}(J' = J + \delta) - \Delta \mathbf{b}_{C_2,GP}(J' = J - \delta)|}{2\delta}, \quad (6)$$

with

$$\Delta \mathbf{b}_{C_2,GP} = \mathbf{b}(J') - \mathbf{b}_{C_2,GP}(J). \quad (7)$$

Clearly, if $\Delta \mathbf{b}$ goes to zero linearly with δ the generalized bond susceptibility is a constant independent of system size and the associated symmetry is not spontaneously

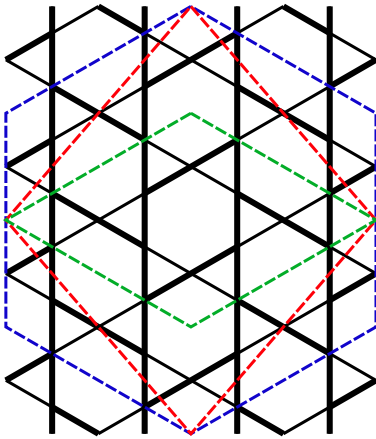


FIG. 5: (Color online.) The 12, 24 and 36 site lattices.

broken. On the other hand, a bond susceptibility diverging with system size signals that the associated symmetry is spontaneously broken in the thermodynamic limit.

When performing exact diagonalization studies of small systems the choice of the finite cluster is crucial since the smaller clusters will reduce the point group symmetry of the infinite lattice. For the isotropic kagomé lattice, $\lambda_D = 1$, the plane group is $p6mm$. This symmetry group implies that for the isotropic kagomé lattice all bonds are equivalent. Our choice of finite clusters are shown in Fig. 5 for $N = 12, 24, 36$. Only the $N = 36$ cluster has the full symmetry point group symmetry of the kagomé lattice. However, for all clusters do we find that all bonds are equivalent at $\lambda_D = 1$. For $0 < \lambda_D < 1$ only two different type of bonds occur for these clusters. These are the only clusters we have found with these properties. For the bond susceptibilities to yield meaningful information about the thermodynamic limit this is very important since we want to make sure that the presence of a reduced point group symmetry doesn't explicitly break the C_2 or GP symmetry. This is not the case for the clusters shown in Fig. 5.

Using the clusters from Fig. 5 we can now study χ_{GP} and χ_{C_2} as a function of λ_D for the different clusters. Our results are shown in Figs 6,7 respectively. We have used $\delta \leq 0.001$ small enough that χ , Eq. (6), is almost completely independent of δ . We begin by discussing χ_{GP} shown in Fig. 6. For λ_D less than roughly ~ 0.8 do we find that χ_{GP} is almost independent of N . In the inset is shown $1/\chi_{GP}$ as a function of $1/N$ for $\lambda = 0.3$ indicating a finite value in the thermodynamic limit. This is consistent with the GP symmetry not being broken. However, for λ_D greater than ~ 0.8 pronounced size dependence occurs. At $\lambda_D = 1$, $1/\chi_{GP}$ as a function of $1/N$ is shown in the inset. In this case it seems reasonable to conclude that χ_{GP} diverges with N and hence that the GP symmetry is spontaneously broken in the thermodynamic limit. A natural interpretation of this result is that a quantum phase transition occurs at ~ 0.8

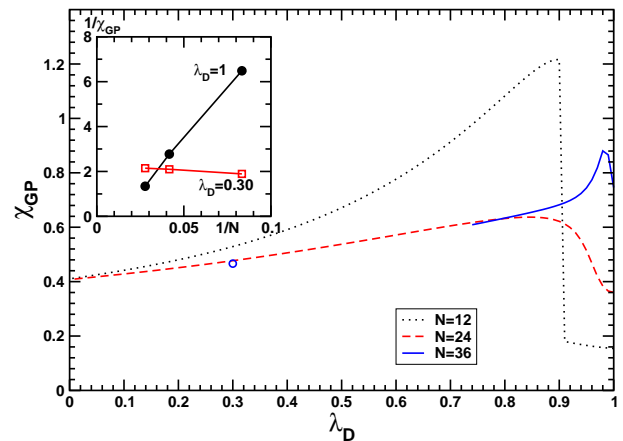


FIG. 6: (Color online.) The glide-plane susceptibility, χ_{GP} as a function of λ_D for the different system sizes, $N = 12, 24, 36$. The circles represent results for $N = 36, \lambda_D = 0.3$. The inset shows χ_{GP}^{-1} versus $1/N$ at $\lambda_D = 0.3, 1.0$.

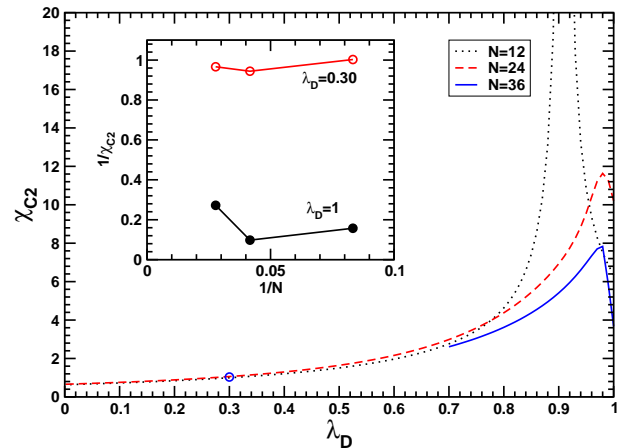


FIG. 7: (Color online.) The C_2 susceptibility, χ_{C_2} as a function of λ_D for the different system sizes, $N = 12, 24, 36$. The circles represent results for $N = 36, \lambda_D = 0.3$. The inset shows χ_{C_2} versus $1/N$ at $\lambda_D = 0.3, 1.0$.

between a state with anti-ferromagnetic order, that does not break the GP symmetry, to a *new* phase where the GP symmetry is *broken*.

Finally, in Fig. 7 we show our results for χ_{C_2} . Again we see that for λ_D smaller than roughly ~ 0.8 there is very little N dependence. In the inset in Fig. 7 is shown $1/\chi_{C_2}$ as a function of $1/N$ at $\lambda_D = 0.3$. Clearly the results extrapolate to a finite value in the thermodynamic limit consistent with the absence of C_2 symmetry breaking as would be the case for an anti-ferromagnetic phase. As before, we find that for λ_D greater than roughly ~ 0.8 pronounced finite size effects occur consistent with a quantum phase transition. However, in this case, as can be seen in the inset in Fig. 7 at $\lambda_D = 1$, the susceptibility *doesn't diverge* but rather tends to a finite, possibly very

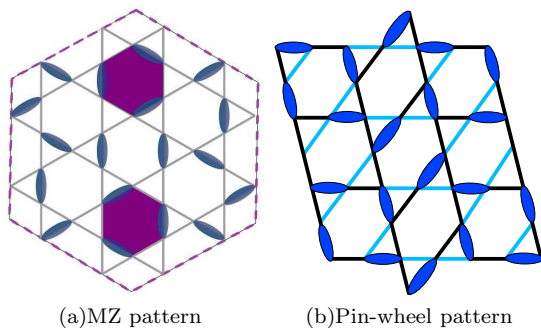


FIG. 8: (a) The Marston and Zeng(MZ) dimer pattern¹⁹ on the kagomé lattice and (b) the pin-wheel state on the distorted kagomé lattice⁹. The MZ pattern arises by maximizing the number of dimers around each hexagon. Notice how the dimers on the two highlighted hexagons can be rotated by 180 about the center of the hexagon without needing to alter the rest of the dimer pattern. This benzene-like resonance suggests that rotational symmetry may be only very weakly broken if this is the ground state. The pin-wheel pattern, on the other hand, maximizes dimers around each rhombus and is manifestly C_2 rotationally symmetric about each hexagon.

small value in the thermodynamic limit. Therefore, in the new phase occurring for λ_D greater than 0.8 the C_2 symmetry is not broken.

IV. DISCUSSION

Given these results, we may draw several conclusions. At $\lambda_D = 0$, we have demonstrated that the spin gap vanishes and that the ground state has a finite staggered magnetization that is 22% smaller than the square lattice value. We find this surprising given that each site has either two or three neighbors (with 2.67 neighbors on average) and that this network is not far from the one dimensional chain model which is disordered. It appears that this form of dimensional reduction does not easily suppress magnetic order.

While we could only study very small system sizes for $\lambda_D > 0$, finite size effects seem to be small all the way out to $\lambda_D \approx 0.8$. As a result, the anti-ferromagnetic order is quite robust and appears to be the ground state with a large basin of stability.

The ground state for $0.8 \lesssim \lambda_D \leq 1$ appears to break the glide plane symmetry while remaining invariant under C_2 rotations. While larger systems would be required to make definitive conclusions, this evidence is in stark contrast to the prediction that the kagomé lattice ground state is a spin liquid^{19,20}.

Remarkably, on this lattice all valence bond crystals break the glide plane symmetry (the most glide-plane symmetric configuration of Fig. 4(b) still breaks glide plane symmetry if the missing dimers are added to the picture). So the breaking of glide plane symmetry strongly supports recent proposals^{1,2,15} that the ground

state maybe a valence bond crystal (VBC). Candidate such states include the Marston and Zeng 36 site unit cell dimer (spin singlet) pattern(MZ)¹⁹ and the pin-wheel pattern (in the presence of distortion) (see Fig. 8). One may argue that the MZ pattern should also break C_2 rotational symmetry. However, such a symmetry may naturally be restored by benzene-like resonances on the three dimer hexagons. One should note that whether the recent ED results¹⁶ are disfavoring the MZ VBC state as well as other proposed VBC states^{1,21} or not, is a subject of intense debate.¹⁵

Since any VBC will have a diverging glide-plane susceptibility the results presented here are not very sensitive to transitions between different VBC's as long as they conserve C_2 symmetry. For example, a transition from the MZ pattern at $\lambda_D = 1$ to the pin-wheel pattern at $\lambda_D < 1$ is certainly possible. For $0.8 \lesssim \lambda_D$ we can therefore not exclude the presence of several different C_2 symmetric VBC phases although the rate of divergence of χ_{GP} could potentially be quite different for different phases. In fact, one might speculate that the cusp in χ_{GP} for $N = 36$ and in χ_{C_2} for $N = 24, 36$ in both cases at $\lambda_D^c = 0.98$ is a signature of a phase-transition between different valence bond crystals.

A phase transition near $\lambda_D \approx 0.8$ was also found in the large-N study of Ref. 9. Thus both large-N and exact diagonalization methods predict the existence of a quantum phases transition at a value of λ_D away from the ideal kagomé limit. If we assume that the spin gap is non-zero at $\lambda_D = 1$ and vanish approximately linearly with the deviation of λ_D from 1, then this value for the quantum critical point is also roughly consistent with the vanishing of the spin gap (which, from exact diagonalizations, is estimated to rather small but finite^{20,22} in the thermodynamic limit and has a value of 0.1848J at $\lambda_D = 1$ for the 36-site cluster). Given the apparent glide plane symmetry breaking for $\lambda_D \gtrsim 0.8$, this phase transition then appears to be between two phases with *unrelated orders*. It may therefore fall into the deconfined universality class¹⁷ if it is not a first order transition.

Acknowledgments

We thank Young Lee and Seung-Hun Lee for useful discussions. This work was supported by the Natural Sciences and Engineering Research Council of Canada (ESS and YBK), the Canadian Foundation for Innovation (ESS), the Canadian Institute for Advanced Research and the Canada Research Chair Program (YBK). ESS gratefully acknowledge the hospitality of the department of physics at the university of Toronto where part of this work was carried out. This work was made possible by the facilities of the Shared Hierarchical Academic Research Computing Network (SHARC-NET:www.sharcnet.ca).

-
- * Electronic address: sorenson@mcmaster.ca
- ¹ P. Nikolic and T. Senthil, *Phys. Rev. B* **68**, 214415 (2003).
- ² R. R. P. Singh and D. A. Huse, *Phys. Rev. B* **76**, 180407(R) (2007).
- ³ Y. Shimizu, K. Miyagawa, K. Kanoda, M. Maesato, and G. Saito, *Phys. Rev. Lett.* **91**, 107001 (2003).
- ⁴ Z. Hiroi, M. Hanawa, N. Kobayashi, M. Nohara, and H. Takagi, *J. Phys. Soc. Jpn.* **70**, 3377 (2001).
- ⁵ J. S. Helton, K. Matan, M. P. Shores, E. A. Nytko, B. M. Bartlett, Y. Yoshida, Y. Takano, A. Suslov, Y. Qiu, J.-H. Chung, et al., *Phys. Rev. Lett.* **98**, 107204 (2007).
- ⁶ Y. Okamoto, M. Nohara, H. Aruga-Katori, and H. Takagi, *Phys. Rev. Lett.* **99**, 137207 (2007).
- ⁷ S.-H. Lee, H. Kikuchi, Y. Qiu, B. Lake, Q. Huang, K. Habicht, and K. Kiefer, *Nature Materials* **AOP** (2007).
- ⁸ J. H. Kim, S. Ji, S.-H. Lee, B. Lake, T. Yildirim, H. Nijiri, K. Habicht, Y. Qiu, and K. Kiefer, unpublished. See arXiv:0806.0767.
- ⁹ M. J. Lawler, L. Fritz, Y. B. Kim, and S. Sachdev, *Physical Review Letters* **100**, 187201 (pages 4) (2008), URL <http://link.aps.org/abstract/PRL/v100/e187201>.
- ¹⁰ M. Rigol and R. R. P. Singh, *Phys. Rev. Lett.* **98**, 207204 (2007).
- ¹¹ M. Tovar, K. S. Raman, and K. Shtengel, *Phys. Rev. B* **79**, 024405 (2009).
- ¹² K. Beach and A. W. Sandvik, *Nuclear Physics B* **750**, 142 (2006), ISSN 0550-3213, URL <http://www.sciencedirect.com/science/article/B6TVC-4K7FFKT-1/2/c97ff1735c126caf67146012a075e6cd>.
- ¹³ A. W. Sandvik, *Physical Review Letters* **95**, 207203 (pages 4) (2005), URL <http://link.aps.org/abstract/PRL/v95/e207203>.
- ¹⁴ A. W. Sandvik, arXiv:0807.0682 (2008).
- ¹⁵ R. R. P. Singh and D. A. Huse, *Physical Review B (Condensed Matter and Materials Physics)* **77**, 144415 (pages 7) (2008), URL <http://link.aps.org/abstract/PRB/v77/e144415>.
- ¹⁶ G. Misguich and P. Sindzingre, *Journal of Physics: Condensed Matter* **19**, 145202 (9pp) (2007), URL <http://stacks.iop.org/0953-8984/19/145202>.
- ¹⁷ T. Senthil, A. Vishwanath, L. Balents, S. Sachdev, and M. P. A. Fisher, *Science* p. 1490 (2004).
- ¹⁸ J. D. Reger and A. P. Young, *Physical Review B (Condensed Matter)* **37**, 5978 (1988), URL <http://link.aps.org/abstract/PRB/v37/p5978>.
- ¹⁹ J. B. Marston and C. Zeng, 35th annual conference on magnetism and magnetic materials **69**, 5962 (1991), URL <http://link.aip.org/link/?JAP/69/5962/1>.
- ²⁰ C. Waldtmann, H.-U. Everts, B. Bernu, C. Lhuillier, P. Sindzingre, P. Lecheminant, and L. Pierre, *The European Physical Journal B* **2**, 501 (1998), URL <http://dx.doi.org/10.1007/s100510050274>.
- ²¹ A. V. Syromyatnikov and S. V. Maleyev, *Phys. Rev. B* **66**, 132408 (2002).
- ²² P. Lecheminant, B. Bernu, C. Lhuillier, L. Pierre, and P. Sindzingre, *Phys. Rev. B* **56**, 2521 (1997).